Journal of Alloys and Compounds, 183 (1992) 413–429
JALCOM 7043

Synthesis, structure and properties of the cluster anions $[(Mo_6Cl_8^i)X_6^a]^{2-}$ with $X^a \equiv F$, Cl, Br, I*

Wilhelm Preetz and Karsten Harder
Institut für Anorganische Chemie der Christian-Albrechts-Universität, Olshausenstrasse 40-60, W-2300 Kiel (FRG)

H. G. von Schnering, Gerhard Kliche and Karl Peters
Max-Planck-Institut für Festkörperforschung, Heisenbergstr. 1, W-7000 Stuttgart 80 (FRG)

(Received January 18, 1992)

Abstract

The tetrabutylammonium (TBA) salts of the octa-μ_3-chloro-hexahalogeno-octahedro-hexamolybdate(2−) ions $[(Mo_6Cl_8^i)X_6^a]^{2-}$ with $X^a \equiv F$, Cl, Br, I were synthesized from the appropriate free acid of the type $H_2[(Mo_6Cl_8^i)X_6^a]$ with $X^a \equiv (BF_4)^-$, Cl^-, Br^-, I^- and the corresponding TBA halide. The crystal structures determined from single crystals show systematic changes in bond distances and angles with the $F^a \rightarrow I^a$ ligand exchange (increasing Mo_6 octahedron; slight compression of the Cl_8^i cube). Infrared and Raman spectra were measured in solution and in the solid state (80 K). The vibrational modes of the cluster kernel $Mo_6Cl_8^i$ are approximately site constant, but all vibrations with contributions of the X^a ligands show characteristic shifts. The most important bands are assigned by use of normal coordinate analyses.

1. Introduction

X-ray structure analyses have been carried out on many molybdenum cluster compounds with the central $Mo_6Cl_8^i$ unit [1–3]. However, the interpretation of the vibrational spectra, which are predominantly based on IR and a few Raman measurements, is contradictory. This is especially true for the assignment of the metal-to-metal vibrations of the Mo_6 octahedron [4–7]. The preparation of single crystals of the tetrabutylammonium (TBA) salts of $[(Mo_6Cl_8^i)X_6^a]^{2-}$ with $X^a \equiv F$, Cl, Br, I now makes available a homologous series of isotypic compounds which allows systematic studies of the influence of the X^a substitution on interatomic distances and vibrational frequencies.

2. Preparation and properties

The preparation of alkylammonium salts $[(Mo_6Cl_8^i)X_6^a]^{2-}$ with $X^a \equiv Cl$, Br, I has already been described in the literature [5]. We modify the procedure

*Dedicated to Professor Ch. J. Raub on the occasion of his 60th birthday.

by taking the molybdenum chloro acid [8] instead of Mo_6Cl_{12} as starting material. On adding a (TBA)Cl surplus to an ethanolic solution, the salt $(TBA)_2[(Mo_6Cl_8^i)Cl_6^a]$ is precipitated quantitatively as a light yellow powder:

$$H_2[(Mo_6Cl_8^i)Cl_6^a] + 2(TBA)Cl \longrightarrow (TBA)_2[(Mo_6Cl_8^i)Cl_6^a]\downarrow + 2HCl \quad (1)$$

To prepare the bromo and iodo compounds, the weakly bound Cl^a ligands are separated as AgCl(s) from the ethanolic solution by adding a stoichiometric amount of $AgBF_4$:

$$H_2[(Mo_6Cl_8^i)Cl_6^a] + 6AgBF_4 \longrightarrow H_2[(Mo_6Cl_8^i)(BF_4)_6] + 6AgCl(s) \quad (2)$$

Solutions of the molybdenum bromo and/or iodo acid yield by addition of a surplus of NaBr and/or NaI, and after addition of the corresponding TBA halides, the light yellow TBA salts, which precipitate quantitatively ($X \equiv Br$, I):

$$H_2[(Mo_6Cl_8^i)(BF_4)_6] + 6NaX \longrightarrow H_2[(Mo_6Cl_8^i)X_6^a] + 6NaBF_4 \quad (3)$$

$$H_2[(Mo_6Cl_8^i)Cl_6^a] + 2(TBA)X \longrightarrow (TBA)_2[(Mo_6Cl_8^i)X_6^a]\downarrow + 2HX \quad (4)$$

Up to now, only the ammonium and caesium salts of the fluoro acid are known [9]. To prepare the TBA salt, a large surplus of solid (TBA)F trihydrate is added to the BF_4^- intermediate (see eqn. (2)). Because of the large solubility in ethanol, one has to evaporate to dryness *in vacuo*. After dissolving with some acetone, complete precipitation of the light yellow $(TBA)_2[(Mo_6Cl_8^i)F_6^a]$ powder results on adding some ether:

$$H_2[(Mo_6Cl_8^i)(BF_4)_6] + 6(TBA)F \longrightarrow (TBA)_2[(Mo_6Cl_8^i)F_6^a]\downarrow + 2HBF_4 + 4(TBA)BF_4 \quad (5)$$

The light yellow solids are not hygroscopic and are stable in air. They increasingly dissolve with the same colour in dichloromethane, acetone and acetonitrile. They are insoluble in water, methanol, ethanol and ether. From saturated solutions (room temperature) of the TBA salt in dichloromethane or acetonitrile, light yellow isometric crystals of up to 1 mm in size crystallize during slow cooling to 5 °C. When placed in mother-lye, these crystals are absolutely transparent, but become dull during washing and drying.

3. Structure investigations

3.1. Crystal structure analysis

All structures were determined on single crystals. The hexachloro and hexabromo compounds crystallize free of solvent molecules and are isotypic. The hexafluoro compound crystallizes with one CH_2Cl_2 molecule and the hexaiodo compound with one CH_3CN molecule per formula unit. The refinement of the data of the hexabromo compound was not quite sufficient (Table 1) because of the poor quality of the crystals (twinning), but this is mostly

TABLE 1

Crystallographic data for $(TBA)_2X$, X ≡ **1**, **2**, **3**, **4**. Compound **1** crystallizes with one CH_2Cl_2 molecule per formula unit, **4** with CH_3CN

	1 $[(Mo_6Cl_8)F_6]^{2-}$	**2** $[(Mo_6Cl_8)Cl_6]^{2-}$	**3** $[(Mo_6Cl_8)Br_6]^{2-}$	**4** $[(Mo_6Cl_8)I_6]^{2-}$
Formula weight	1458.20 + 84.93	1556.93	1823.10	2105.63 + 41.05
Crystal size (mm^3)	0.75 × 1.0 × 0.4	0.25 × 0.3 × 0.1	0.1 × 0.15 × 0.05	0.2 × 0.3 × 0.15
Space group (no.)	*Pbca* (61)	$P2_1/n$ (14)	$P2_1/n$ (14)	$C2/m$ (12)
Lattice constants at 298 K: *a* (pm)	1762.6(5)	1849.0(4)	1877.2(9)	1758.7(2)
b (pm)	2083.7(9)	1166.3(2)	1199.3(7)	2074.0(3)
c (pm)	1568.2(5)	1276.4(3)	1295.7(8)	1176.0(1)
β (deg)	–	90.14(2)	90.57(4)	128.66(1)
Volume ($Å^3$)	5760(4)	2753(1)	2917(3)	3349.5(7)
Molecular volume (cm^{-3} mol^{-1})	867.3(7)	829.1(3)	878.5(7)	1008.7(2)
Molecules per cell, *z*	4	2	2	2
Calculated density (g cm^{-3})	1.779	1.878	2.075	2.128
F(000)	3048	1536	1644	2012
μ (mm^{-1})	1.85	2.01	5.68	4.15
Measurement	Siemens R3m/V four-circle diffractometer; Mo Kα, monochromator graphite; $1.75° \leqslant \theta \leqslant 27.5°$; Wyckoff scan, 1.5–19.5 deg min^{-1}			
Structure determination	Progamme system SHELXTL-PLUS; empirical absorption correction; direct phase determination, $E_{min} = 1.2$; full matrix least-squares; MICROVAX II			
$N(hkl)$; $N(F \geqslant 3\sigma(F))$	5097; 4266	4882; 3760	6698; 2368	3067; 2595
R (anisotropic) (H isotropic)	0.045	0.048	0.149	0.037

reflected in the parameters of the cations and therefore we finished the work at this stage. Crystallographic data and details of the structure determination are compiled in Table 1. Tables 2–5 contain the atomic parameters and Table 6 the most important interatomic distances and angles. Figure 1 shows the anions with the atomic labelling. Further details on the crystal structure investigation are available on request from the Fachinformationszentrum Karlsruhe, Gesellschaft für wissenschaftlich technische Information m.b.H., W-7514 Eggenstein-Leopoldshafen 2, FRG on quoting the depository number CSD-56251, the names of the authors and the journal citation.

TABLE 2

$(TBA)_2[(Mo_6Cl_8^i)F_6^a]\cdot CH_2Cl_2$ (**1**): positional parameters ($\times 10^4$) and mean displacement parameters U_{eq} ($pm^2 \times 10^{-1}$); standard deviations in parentheses

	x	y	z	U_{eq}
Mo(1)	368(1)	5677(1)	9377(1)	41(1)
Mo(2)	749(1)	4487(1)	9566(1)	43(1)
Mo(3)	−623(1)	4776(1)	9111(1)	44(1)
Cl(1)	230(1)	6358(1)	10664(1)	64(1)
Cl(2)	1671(1)	5369(1)	9846(1)	56(1)
Cl(3)	−960(1)	5931(1)	8968(1)	61(1)
Cl(4)	471(1)	4941(1)	8134(1)	58(1)
F(1)	772(2)	6410(2)	8705(2)	66(1)
F(2)	1574(2)	3949(2)	9061(3)	75(2)
F(3)	−1293(2)	4523(2)	8144(2)	78(2)
N(1)	3605(3)	1629(3)	4428(3)	49(2)
C(2)	2919(4)	2027(3)	4210(4)	54(2)
C(3)	2879(4)	2691(3)	4615(5)	65(3)
C(4)	2116(4)	3005(3)	4388(5)	72(3)
C(5)	1437(4)	2687(4)	4780(5)	79(3)
C(6)	4334(4)	1935(3)	4091(5)	66(3)
C(7)	4378(5)	2063(4)	3166(5)	84(3)
C(8)	5181(6)	2309(5)	2974(7)	134(6)
C(9)	5323(7)	2589(6)	2267(6)	172(8)
C(10)	3472(4)	978(3)	4002(4)	52(2)
C(11)	4069(4)	475(3)	4150(5)	62(3)
C(12)	3828(4)	−152(3)	3761(4)	64(3)
C(13)	4410(5)	−681(4)	3862(5)	86(4)
C(14)	3717(4)	1559(4)	5376(4)	60(3)
C(15)	3074(4)	1268(4)	5869(4)	72(3)
C(16)	3274(5)	1251(5)	6803(5)	91(4)
C(17)	2692(5)	977(5)	7365(5)	117(5)
Cl(5)	1457(2)	730(1)	1222(2)	103(1)
Cl(6)	2369(2)	1775(1)	1885(2)	119(1)
C(1)	2076(5)	986(4)	2028(5)	83(3)

TABLE 3

$(TBA)_2[(Mo_6Cl_8^i)Cl_6^a]$ (**2**): positional parameters ($\times 10^4$) and mean displacement parameters U_{eq} ($pm^2 \times 10^{-1}$); standard deviations in parentheses

	x	y	z	U_{eq}
Mo(1)	5193(1)	533(1)	8673(1)	44(1)
Mo(2)	5847(1)	639(1)	10482(1)	43(1)
Mo(3)	5484(1)	−1339(1)	9695(1)	43(1)
Cl(1)	4837(1)	−1371(2)	8002(1)	58(1)
Cl(2)	5529(1)	2382(2)	9484(2)	57(1)
Cl(3)	3924(1)	1181(2)	8571(1)	52(1)
Cl(4)	6445(1)	−141(2)	8918(1)	55(1)
Cl(5)	6962(1)	1462(2)	11132(2)	65(1)
Cl(6)	5429(1)	1183(2)	6903(2)	77(1)
Cl(7)	6124(1)	−3078(2)	9254(2)	73(1)
N(1)	7913(3)	4750(5)	272(4)	56(2)
C(2)	8061(4)	6023(7)	41(6)	65(3)
C(3)	8548(4)	6632(7)	808(6)	70(3)
C(4)	8625(5)	7874(8)	513(8)	82(4)
C(5)	7950(5)	8555(8)	595(9)	115(5)
C(6)	7602(4)	4592(7)	1353(5)	64(3)
C(7)	6908(4)	5234(8)	1604(7)	76(3)
C(8)	6249(6)	4590(9)	1613(10)	120(6)
C(9)	5622(6)	5196(10)	2029(9)	135(6)
C(10)	7372(4)	4301(8)	−518(6)	68(3)
C(11)	7605(5)	4351(11)	−1639(6)	112(5)
C(12)	6899(7)	3995(10)	−2420(10)	142(4)
C(13)	7121(8)	2954(11)	−2356(12)	188(7)
C(14)	8631(4)	4126(8)	192(7)	76(4)
C(15)	8618(5)	2864(9)	256(9)	108(5)
C(16)	9289(6)	2323(10)	−164(12)	126(6)
C(17)	9308(8)	1269(14)	−374(15)	284(15)

3.2. Discussion

The real point symmetry of the cluster anions in the crystals is only $\bar{1}$ with the F^a, Cl^a and Br^a compounds but $2/m$ with I^a. However, independently of the quite different structure types, the central cluster cage $Mo_6Cl_8^i$ exhibits $m\bar{3}m$–O_h symmetry within the error limits. Larger deviations occur with the large extending X_6^a octahedra, which may be affected by the molecular packing. Therefore we compiled the mean $m\bar{3}m$ values in Table 6 for further discussion.

It has been known for a long time that metal-to-metal bond lengths are strongly influenced by the size of the surrounding ligand sphere [1, 14]. This is reflected with the $[(Mo_6X_8^i)X_6^a]^{2-}$ and $[(W_6X_8^i)X_6^a]^{2-}$ cluster units in the series X≡O, Cl, Br, I (Table 6 and ref. 13), where the bond lengths d_{Mo-Mo} and/or d_{W-W} are 2.536 Å (X≡O), 2.602 or 2.607 Å (X≡Cl), 2.640 or 2.635 Å (X≡Br) and 2.671 Å (X≡I) respectively. Furthermore, the square MX_4^i units are not almost planar and therefore the M–X^i distance is not the

TABLE 4

$(TBA)_2[(Mo_6Cl_8^i)Br_6^a]$ (3): positional parameters ($\times 10^4$) and mean displacement parameters U_{eq} ($pm^2 \times 10^{-1}$); standard deviations in parentheses

	x	y	z	U_{eq}
Mo(1)	5155(2)	579(3)	8706(2)	49(1)
Mo(2)	5848(2)	597(3)	10459(2)	45(1)
Mo(3)	5468(2)	−1288(3)	9628(2)	50(1)
Cl(1)	4784(5)	−1237(10)	7998(7)	71(4)
Cl(2)	5506(5)	2333(9)	9547(8)	72(4)
Cl(3)	3900(5)	1195(9)	8705(7)	65(4)
Cl(4)	6399(4)	−87(9)	8859(6)	66(4)
Br(5)	7032(2)	1410(4)	11121(3)	72(2)
Br(6)	5348(2)	1332(5)	6881(3)	90(2)
Br(7)	6118(2)	−3060(4)	9044(3)	92(2)
N(1)	7924(15)	4735(29)	184(22)	75(15)
C(2)	8065(20)	5991(32)	15(27)	77(13)
C(3)	8517(21)	6591(36)	796(29)	106(16)
C(4)	8612(22)	7751(36)	578(31)	101(15)
C(5)	8004(26)	8367(41)	555(34)	172(24)
C(6)	7618(20)	4565(35)	1233(27)	86(13)
C(7)	6962(24)	5111(39)	1519(33)	117(17)
C(8)	6286(31)	4620(52)	1587(43)	210(29)
C(9)	5722(25)	5149(47)	2092(38)	192(26)
C(10)	7402(19)	4325(35)	−603(27)	86(13)
C(11)	7536(23)	4417(43)	−1666(30)	136(19)
C(12)	6771(33)	4038(50)	−2467(45)	241(33)
C(13)	7090(37)	3061(51)	−2339(51)	284(44)
C(14)	8647(23)	4164(37)	70(32)	109(17)
C(15)	8629(25)	3014(41)	108(33)	129(19)
C(16)	9293(25)	2406(38)	−404(34)	135(19)
C(17)	9242(30)	1266(46)	−457(41)	224(30)

only important parameter in assessing the relative strength of the interaction (as stated in ref. 13). An $M_6X_8^i$ cage with square planar MX_4^i units is characterized by an angle $M\text{–}X^i\text{–}M = 60°$ and by $2\Delta = 2^{1/2}d_{MM} - d(X^i\text{–}X^i) = 0$. If the M_6 octahedron extends the X_8^i cube, then $\Delta > 0$ and $\alpha > 60°$ and vice versa, making these values appropriate to measure the deviation from MX_4^i planarity. The values $\Delta^* = d(X^i\text{–}X^a) - \Sigma R(X_{i,a}^-)$ and $Q = d(X^i\text{–}X^i)/2R(X_i^-)$ may be taken as measures of the repulsive interactions $X^i\text{–}X^a$ and $X^i\text{–}X^i$ (see Table 6). In the series $X^{i,a} \equiv$ O, Cl, Br, I one observes (tungsten compound) $\Delta = +0.268$, $+0.095(+0.077)$, $+0.038(+0.005)$, (-0.085) Å and $\alpha = 71.4°$, 63.6° (62.9°), 61.4° (60.2°), (57.2°). In other words, only the bromo cluster exhibits more or less planar MX_4^i squares. The values $Q = 1.09$, 0.96 (0.98), 0.94 (0.95), (0.90) demonstrate increasing relative compression of the X_8^i cube due to the strong $M\text{–}X^i$ bonds, which also give rise to the *absolute increase* (d_{MM}) but *relative decrease* (Δ) in the M_6 octahedron with increasing size of X. Finally, the values $\Delta^* = +0.43$, -0.10 (-0.09), -0.20 (-0.21), (-0.48) Å show how the external X^a

TABLE 5

$(TBA)_2[(Mo_6Cl_8^i)I_6^a] \cdot CH_3CN$ (**4**): positional parameters ($\times 10^4$) and mean displacement parameters U_{eq} ($pm^2 \times 10^{-1}$); standard deviations in parentheses

	x	y	z	U_{eq}
Mo(1)	3847(1)	0	3108(1)	45(1)
Mo(2)	4507(1)	631(1)	5489(1)	45(1)
I(1)	3782(1)	−1580(1)	6257(1)	70(1)
I(2)	2129(1)	0	233(1)	73(1)
Cl(1)	2986(1)	0	4143(2)	52(1)
Cl(2)	6090(1)	1188(1)	6786(2)	55(1)
Cl(3)	4849(2)	0	2304(2)	55(1)
N(1)	0	1612(4)	5000	62(5)
C(2)	−850(4)	2048(3)	3913(7)	67(4)
C(3)	−1785(4)	1719(3)	2707(7)	77(5)
C(4)	−2541(5)	2213(4)	1693(8)	99(6)
C(5)	−3496(5)	1937(5)	422(8)	117(6)
C(6)	245(5)	1171(3)	4229(8)	71(5)
C(7)	557(5)	1503(4)	3431(8)	82(5)
C(8)	745(5)	1024(4)	2675(8)	89(5)
C(9)	1123(6)	1319(5)	1969(8)	112(6)
C(10)	7347(11)	0	2750(14)	107(10)
C(11)	6385(9)	0	1404(13)	130(10)
N(12)	8112(11)	0	3773(14)	193(11)

ligands try to follow the escaping metal atoms and how strongly the attractive M–X^a bonds may be countered by the repulsive X^i–X^a interactions. The result is that the expected relation $d(M–X^a) < d(M–X^i)$ is reached only with smaller $X^{i,a}$ ligands, which is shown by the mean ratio of the two distances: 0.98, 0.98, 1.00, 1.02.

In the compounds with the $[(Mo_6Cl_8^i)X_6^a]^{2-}$ anions one observes in principle the same but not as pronounced tendencies as follows.

(a) The Cl_8^i cube becomes slightly smaller with $F^a \rightarrow I^a$ (d = 3.52, 3.49, 3.48, 3.48 Å) and $d(Cl^i–Cl^i)$ is about 3%–4% smaller than the anion radii. In other words, the internal compression of the Cl_8^i cube increases slightly (see Q in Table 6).

(b) The Mo_6 octahedron becomes larger with $F^a \rightarrow I^a$ (2.593, 2.602, 2.604, 2.615 Å).

(c) The Δ^* values (+0.06, −0.10, −0.13, −0.21 Å) show that only the F^a compound is free of strain with respect to X^i-to-X^i repulsive interactions and that these interactions become more and more pronounced with $F^a \rightarrow I^a$.

The effects (a) and (b) are also reflected in the changes in the angle Mo–Cl^i–Mo (62.8°, 63.6°, 63.8°, 64.1°) and in Δ (0.075, 0.095, 0.100, 0.107 Å).

Altogether, one has the impression of a relatively soft $M_6X_8^i$ unit, where also the rigidity of the *planar* Mo–Cl^i coordination is not very strong. The refined $MoCl_2$ data [11] demonstrate this relative softness especially in the $d_{Mo–Mo}$ and d(Mo–Cl^i) distances, which obviously depend on the different

TABLE 6

Selected mean interatomic distances (Å) and angles (deg) in $(Mo_6X^i_8)X^a_6$ and $(W_6X^i_8)X^a_6$ clusters; standard deviations in parentheses; $R(X^-)$ are the anion radii and $\Sigma R(X^-)$ their sums

X^i: X^a:	Mo O^i O^a	Mo Cl^i O^a	Mo Cl^i F^a	Mo Cl^i Cl^a	$MoCl^i$ † $2Cl^a$, $4Cl^{a-a}$	$MoCl^i$ Br^a	Mo Cl^i I^a	Mo Br^i Br^a	W Cl^i Cl^a	W Br^i Br^a	W I^i I^a
d(M–M)	2.536(8)	2.607(4)	2.593(5)	2.602(4)	2.608(1) 8× 2.604(1) 4×	2.604(4)	2.615(2)	2.640(2)	2.607	2.635	2.671
d(M–X^i)	2.173(13)	2.490(6)	2.488(2)	2.469(5)	2.474(1) 8× 2.469(2) 16×	2.465(9)	2.466(4)	2.587(2)	2.499	2.628	2.792
d(M–X^a)	2.130(38)	2.051(29)	1.993(7)	2.420(4)	2.379(3) 2× 2.494(1) 4×	2.565(4)	2.788(5)	2.606(2)	2.416	2.587	2.839
M–X^i–M	71.4	63.0	62.8	63.6	63.7	63.8	64.1	61.4	62.9	60.2	57.2
d(X^i–X^i)	3.050	3.522	3.517	3.489	3.482 4× 3.495 8×	3.483	3.484	3.658	3.532	3.717	3.947
d(X^i–X^a)	3.225	3.289	3.234	3.523	3.496^a 3.579^{a-a}	3.629	3.801	3.699	3.530	3.692	3.920
Δ	+0.268	+0.082	+0.075	+0.095	+0.106 +0.094	+0.100	+0.107	+0.038	+0.077	+0.005	−0.085
$\Sigma R(X^-_{i,a})$	2.80	3.21	3.17	3.62	3.62	3.76	4.01	3.90	3.62	3.90	4.40
Δ*	+0.43	+0.08	+0.06	−0.10	$-0.12^{(a)}$ $-0.04^{(a-a)}$	−0.13	−0.21	−0.20	−0.09	−0.21	−0.48
Q	1.09	0.97	0.97	0.96	0.96	0.96	0.96	0.94	0.98	0.95	0.90
Reference	[10]	[10]	–	–	[11]	–	–	[12]	[13]	[13]	[13]

Definitions: $2\Delta = 2^{1/2}d(M–M) - d(X^i–X^i)$; $\Delta^* = d(X^i–X^a) - \Sigma R(X^-_{i,a})$; $Q = d(X^i–X^i)/2R(X^-_i)$.

†Data of the refined $MoCl_2$ structure [11].

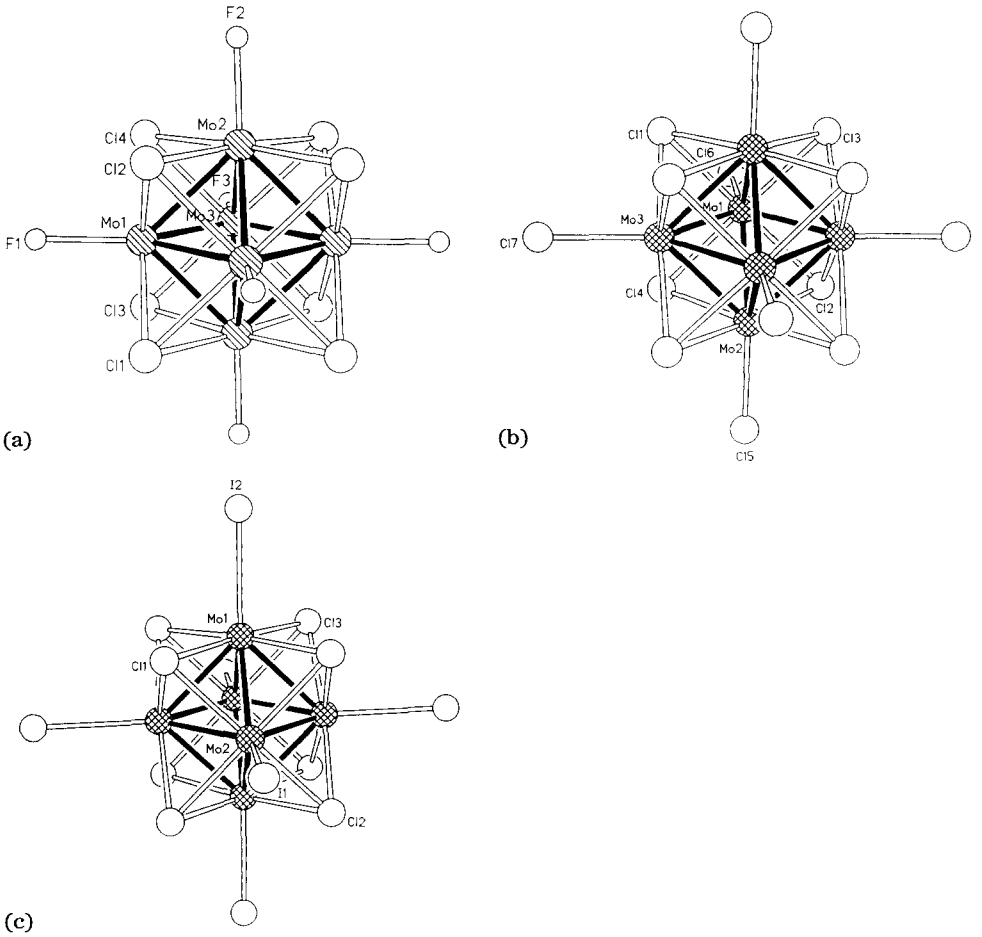

Fig. 1. Cluster anions $[Mo_6Cl_8^i)X_6^a]^{2-}$ and atomic labelling for $X^a \equiv$ (a) F, (b) Cl, (c) I (see Tables 2–5).

distances $d(Mo–Cl^a) \neq d(Mo–Cl^{a-a})$ (Cl^{a-a} are bridging outer ligands). Where $d(Mo–Cl^a)$ becomes smaller, the Mo_6 octahedron is stretched and the Cl_8^i cube is compressed, *e.g.* Δ becomes larger (see the I^a complex in Table 6). Simultaneously Δ^* becomes more pronouncedly negative, corresponding to the more compressed X^i–X^a region. Finally, the difference in the $d(Mo–Cl^a)$ values of the neutral $MoCl_2$ (2.379 Å) and the charged anion (2.420 Å) should be mentioned.

There is no doubt that pure steric factors as well as electronic interactions [13] contribute to the structural changes and it is not easy to separate these contributions, which very often go in parallel. Recently published nuclear magnetic resonance (NMR) studies [15] may be very helpful. The ^{95}Mo resonance signal of the F^a compound is located at the lowest field and thus indicates the lowest electron density in the Mo_6 octahedron. Corresponding

to the increasing polarizability in the series $Cl^a < Br^a < I^a$, a high field shift is observed, which indicates an increasing electron density in the Mo_6 cage. One may assume an increasing occupation of antibonding Mo_6 orbitals because of the parallel bond length expansion. The decreasing ligand field strength from F^a to I^a will reduce the HOMO–LUMO distances [16] and therefore the decreasing bond strength should mainly result from the increasing participation of antibonding cluster orbitals.

4. Vibrational spectra

4.1. Infrared spectra, Raman spectra

The normal vibrations of the cluster anions $[(Mo_6Cl_8^i)X_6^a]^{2-}$ ($X^a \equiv F$, Cl, Br, I) with the symmetry O_h–$m\bar{3}m$ are represented by the following terms:

$$\Gamma_{Cl^i} = A_{1g} + E_g + T_{1g} + 2T_{2g} + A_{2u} + E_u + 2T_{1u} + T_{2u}$$

$$\Gamma_{Mo} = A_{1g} + E_g + T_{1g} + T_{2g} + 2T_{1u} + T_{2u}$$

$$\Gamma_{X^a} = A_{1g} + E_g + T_{1g} + T_{2g} + 2T_{1u} + T_{2u}$$

$$\Gamma_{Mo_6Cl_8^iX_6^a} = 3A_{1g} + 3E_g + 3T_{1g} + 4T_{2g} + A_{2u} + E_u + 6T_{1u} + 3T_{2u}$$

After elimination of the rotational T_{1g} and translational T_{1u} terms, the internal vibrations of the cluster anions are

$$\Gamma^{vib}_{Mo_6Cl_8^iX_6^a} = 3A_{1g} + 3E_g + 2T_{1g} + 4T_{2g} + A_{2u} + E_u + 5T_{1u} + 3T_{2u}$$

According to the selection rules, the five normal vibrations of T_{1u} symmetry are IR active and the 10 vibrational modes of symmetry A_{1g}, E_g and T_{2g} are Raman active; all the others are inactive.

The IR and Raman spectra of the cluster compounds $(TBA)_2[(Mo_6Cl_8^i)X_6^a]$, $X \equiv F$, Cl, Br, I, are shown in Fig. 2 with the frequencies and labelling of the most important bands. The high symmetry of the cluster anions is reflected in the clearly arranged vibrational spectra. Despite the complicated crystal structures, factor group splittings and positional group splittings are not detectable.

The interpretation of the spectra may start with the assumption that those vibrations which appear at approximately constant frequencies are due to the invariant double-cage system $Mo_6Cl_8^i$, whereas the vibrations that include participation of the external halogen ligands X^a should show characteristic shifts. For the band-rich Raman spectra it is important that the detection of the total symmetrical stretching vibrations of A_{1g} symmetry is made possible through measurements of the depolarization order in concentrated solutions of the TBA salts in propylene carbonate. Figure 3 shows the four most important vibrational modes.

The antisymmetric Mo–X^a stretching mode ν_{14} is clearly recognized as an intensive band in the IR spectra. This band is strongly shifted to higher wavenumbers with decreasing mass of the ligands. A further vibration ν_{15}, which also depends on the mass of the ligands, results from the deformation

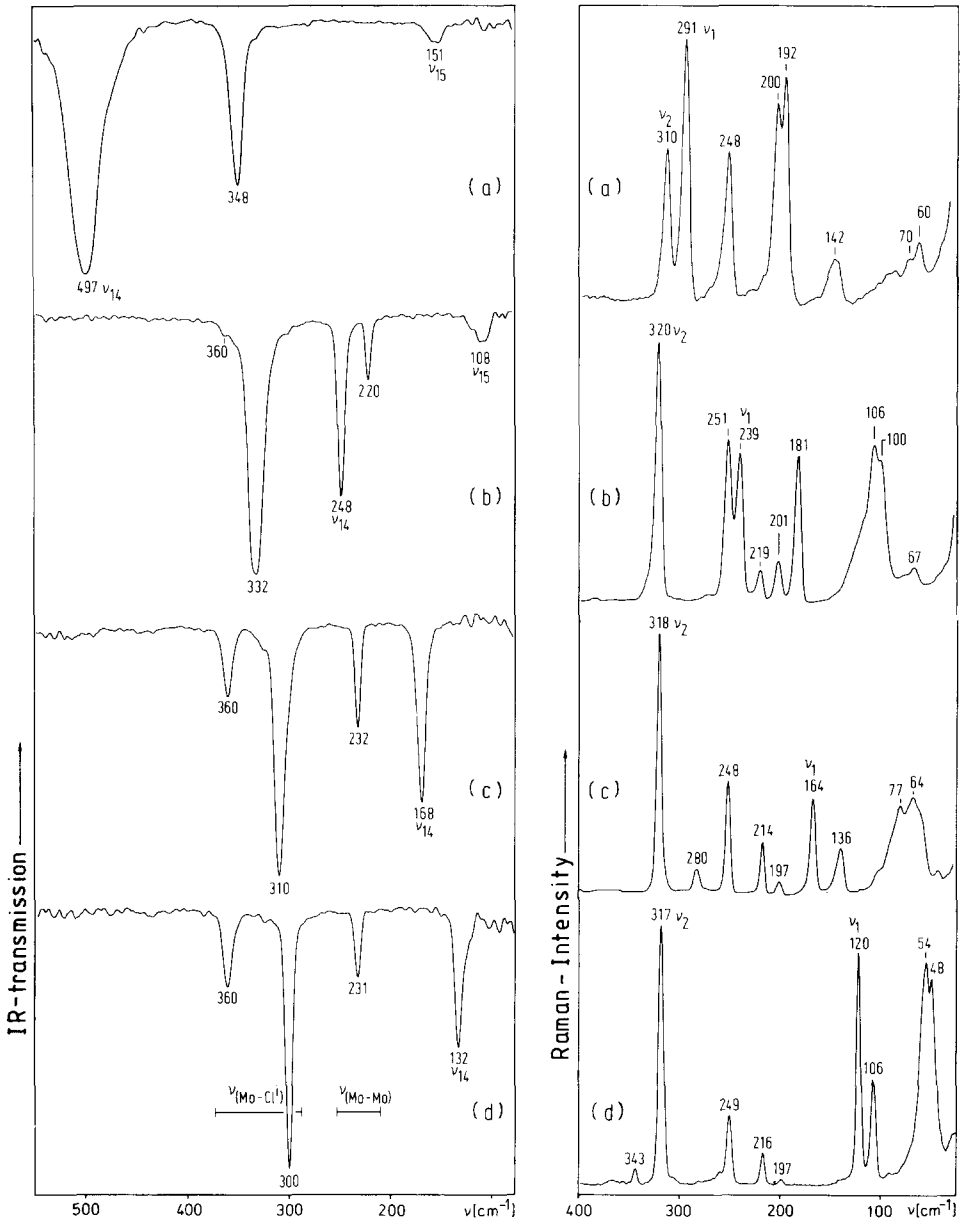

Fig. 2. Infrared (left) and Raman (right) spectra at 80 K of $(TBA)_2[Mo_6Cl_8^i)X_6^a]$, X^a=(a) F, (b) Cl, (c) Br, (d) I; λ_0=514.5 nm.

of the Cl^i–Mo–X^a angle. The corresponding bands are observed at 151 cm^{-1} with the fluoride and at 108 cm^{-1} with the chloride. With the bromide and iodide this band must be located below the measuring range. The remaining bands in the ranges 360, 300–348 and 220–231 cm^{-1} can be assigned to the internal vibrations of the $Mo_6Cl_8^i$ unit [5]. The distinct shift of the most

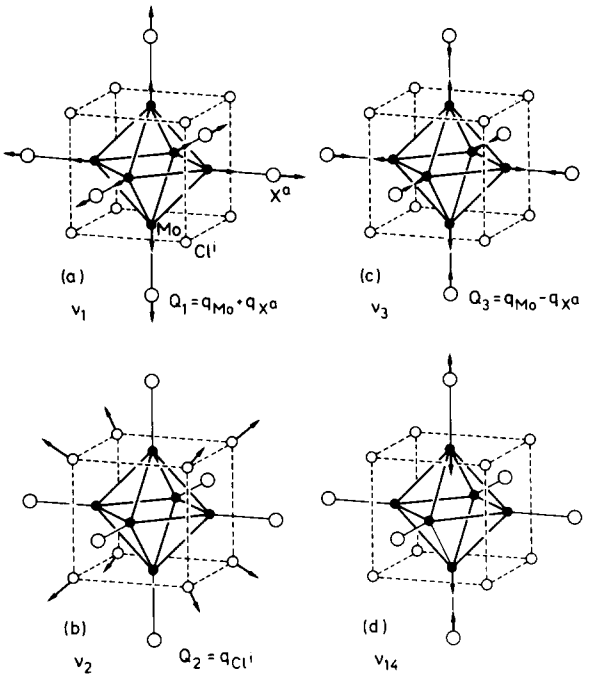

Fig. 3. Stretching modes ν_1, ν_2, ν_3 (A_{1g}) and $\nu_{14}(T_{1u})$ of the cluster anions $[Mo_6Cl^i_8)X^a_6]^{2-}$.

intensive band from 300 to 348 cm^{-1}, which is related to the X^a mass, points towards a considerable vibrational coupling of the double cage $Mo_6Cl^i_8$ with the outer substituents X^a. The large intensity of the band at 230 cm^{-1} speaks against an assignment as a pure metal-to-metal vibration, but indicates considerable contributions of Cl^i and X^a.

The Raman spectra of the solutions of all four compounds show only *two* totally polarized bands instead of the three expected ones. The approximately site-constant strong maximum which appears between 310 and 320 cm^{-1} is assigned to the breathing mode ν_2 of the $Mo_6Cl^i_8$ group (Fig. 3). The second band, which disappears completely with perpendicular polarization, clearly refers to the total symmetric vibration ν_1 with contributions from the terminal X^a ligands because of the strong shift with changing X^a. The absence of the third completely polarized band is due to a vibrational coupling, as already discussed in the related cluster compounds Nb_6F_{15} [17]. While for $^3_\infty[(Nb_6F^i_{12})F^{a-a}_{6/2}]$ an in-phase motion and/or a counterphase motion of the Nb_6 octahedron and the F^i_{12} cuboctahedron were taken into account, corresponding in-phase and/or counterphase vibrations of the stacked Mo_6 and X^a_6 octahedra have to be taken into account in the case of the $(Mo_6Cl^i_8)X^a_6$ system. A high intensity is expected for the in-phase vibration

$$Q_1 = q_{Mo} + q_{X^a} \equiv \nu_1(A_{1g})$$

where q_{Mo} and q_{X^a} define the A_{1g} symmetry coordinates of the Mo_6 and X^a_6 octahedra. A low intensity is expected, on the other hand, for the

counterphase vibration

$$Q_3 = q_{Mo} - q_{X^a} \equiv \nu_3(A_{1g})$$

because of the antiphase components of the polarizability change. The breathing mode ν_2 of the $Mo_6Cl_8^i$ group is regarded as being independent of the X^a ligand and is described as

$$Q_2 = q_{Cl^i} \equiv \nu_2(A_{1g})$$

4.2. Normal coordinate analysis

For the assignment of the Raman bands measured on $H_2[(Mo_6Cl_8^i)Cl_6^a]$, Hartley and Ware [7] have calculated the following frequencies by application of a simple valence force field model with $f_r = f(Mo\text{–}Cl^i) = 1.1$ mdyn Å^{-1}, $f_s = f(Mo\text{–}Mo) = 1.6$ mdyn Å^{-1} and $f_t = f(Mo\text{–}Cl^a) = 1.8$ mdyn Å^{-1}:

$\nu_1(q_{Mo} + q_{Cl^a}) = 236$ cm^{-1} (239 cm^{-1})

$\nu_2(q_{Cl^i}) = 318$ cm^{-1} (320 cm^{-1})

$\nu_3(q_{Mo} - q_{Cl^a}) = 402$ cm^{-1}

The frequencies are in good agreement with the experimental values of ν_1 and ν_2 (in parentheses). For the IR-active vibrations ν_{14} this model yields values which are too high. It seems to be more favourable to follow the more detailed analysis of Mattes [4]. This procedure includes interaction force field constants f_{st}, and allows more accurate calculations of the frequencies ν_1, ν_3 and ν_{14}. The force constants for $X^a \equiv Cl$, Br, I are taken from ref. 4. For $X^a \equiv F$ the following values were determined by fitting $\nu_{14}^{obs} = 497$ cm^{-1}:

$f_s = 1.30$ mdyn Å^{-1}

$f_t = 2.38$ mdyn Å^{-1}

$f_{st} = 0.46$ mdyn Å^{-1}

The calculated ν_1 and ν_3 frequencies as well as the potential energy distribution (PED) are shown in Table 7. While the calculated ν_1 frequencies fit the experimental values quite well, the counterphase vibrations ν_3 are not observed. Indeed, the bromo compound shows a weak band at 280 cm^{-1}; however, because of the small intensity, its polarization behaviour could not be measured.

From the PED it follows that the ν_1 band of the Raman spectra corresponds to an Mo–Mo vibration for $X^a \equiv F$, but that this vibration is a strongly mixed one for $X^a \equiv Cl$ and finally corresponds to a pure Mo–X^a vibration for $X^a \equiv I$.

Independently of the calculations, which only consider total symmetrical vibrations, one can conclude from the Raman spectra that the bands which are practically site constant and of medium and lower intensities (248–251, 214–219 and 197–201 cm^{-1}) must be assigned to the $Mo_6Cl_8^i$ cluster just as for ν_2. They probably belong to the E_g and T_{2g} modes of this group. This

TABLE 7

Measured and calculated frequencies (cm^{-1}), potential energy distribution (PED) (%) and force constants f_s, f_t, f_{st} (mdyn $Å^{-1}$) for $[(Mo_6Cl_8^i)X_6^a]^{2-}$, $X^a \equiv F$, Cl, Br, I; force constants for $X^a \equiv Cl$, Br, I according to ref. 4

X^a	ν_1(exp.)	ν_1(calc.)	ν_3(exp.)	ν_3(calc.)	f_s	f_t	f_{st}	PED, ν_1			PED, ν_3		
								(f_s)	(f_t)	(f_{st})	(f_s)	(f_t)	(f_{st})
F	294	277	–	488	1.3	2.38	0.46	101	0	−1	6	107	−13
Cl	240	232	–	297	1.2	1.30	0.40	38	37	24	72	73	−46
Br	166	157	280	284	1.2	1.23	0.38	9	75	16	102	36	−39
I	121	121	–	284	1.2	1.15	0.36	6	81	13	104	30	−34

experimental result agrees with the model, according to which the vibrations of the $Mo_6Cl_8^i$ unit are mostly independent of the X^a ligands.

A complete normal coordinate analysis including the E_g, T_{2g} and T_{1u} modes is not yet possible because of the large number of interatomic force constants and their numerous interactions. Further investigations are necessary to extend the experimental data, especially those for molybdenum isotopes as well as those for $[(Mo_6Br_8^i)X_6^a]^{2-}$ cluster compounds.

5. Experimental details

The starting material for the synthesis of compounds **1–4** was the molybdenum chloro acid $(H_3O)_2[(Mo_6Cl_8^i)Cl_6^a]\cdot 6H_2O$ [8]. It was prepared by boiling a mixture of an ethanolic solution of $MoCl_2$ ($\equiv Mo_6Cl_{12}$) [18] and conc. HCl.

5.1. Preparation of $(TBA)_2[(Mo_6Cl_8^i)Cl_6^a]$

To a solution of 500 mg (0.41 mmol) $(H_3O)_2[(Mo_6Cl_8^i)Cl_6^a]\cdot 6H_2O$ in 20 ml absolute ethanol an ethanolic solution of 285 mg (2.5×0.41 mmol) (TBA)Cl was added. The precipitation yielded 95% light yellow $(TBA)_2[(Mo_6Cl_8^i)Cl_6^a]$.

5.2. Preparation of $(TBA)_2[(Mo_6Cl_8^i)Br_6^a]$ and $(TBA)_2[(Mo_6Cl_8^i)I_6^a]$

A solution of 300 mg (0.25 mmol) $(H_3O)_2[(Mo_6Cl_8^i)Cl_6^a]\cdot 6H_2O$ in 20 ml absolute ethanol was charged with a solution of 315 mg (6×0.25 mmol + 10%) $AgBF_4$ in 5 ml absolute ethanol. Precipitated AgCl was removed and finely pulverized NaBr (455 mg, 18×0.25 mmol) or NaI (655 mg, 18×0.25 mmol) was added and the mixture stirred for 2 h. The sodium halides were dissolved. Reprecipitated silver halides as well as excess sodium halides caused a cloudiness and were removed by centrifuging. After adding 240 mg (3×0.25 mmol) (TBA)Br or 275 mg (3×0.25 mmol) (TBA)I dissolved in 5 ml absolute ethanol, $(TBA)_2[(Mo_6Cl_8^i)Br_6^a]$ or $(TBA)_2[(Mo_6Cl_8^i)I_6^a]$ precipitation resulted in a 95% yield of a light yellow crystalline powder.

5.3. Preparation of $(TBA)_2[Mo_6Cl_8^i)F_6^a]$

An ethanolic solution of 300 mg (0.25 mmol) $(H_3O)_2[(Mo_6Cl_8^i)Cl_6^a]\cdot 6H_2O$ was charged with 315 mg (6×0.25 mmol + 10%) $AgBF_4$. After separation of AgCl, 1400 mg (18×0.25 mmol) solid $(TBA)F\cdot 3H_2O$ was added and the mixture was stirred for 2 h in a Teflon beaker. Subsequently the batch was completely evaporated in a desiccator over KOH, dissolved in 10 ml acetone and purified from insoluble residues (excess $AgBF_4$) by centrifuging. After addition of ether, light yellow $(TBA)_2[(Mo_6Cl_8^i)F_6^a]$ was precipitated with a 95% yield. All TBA compounds were recrystallized from dichloromethane–ether.

5.4. Analysis

		C (%)	H (%)	N (%)	Cl (%)	Br (%)	I (%)
$(TBA)_2[(Mo_6Cl_8^i)F_6^a]$	calc.	26.35	4.97	1.92	19.45	–	–
	obs.	26.46	5.08	1.96	19.30	–	–
$(TBA)_2[(Mo_6Cl_8^i)Cl_6^a]$	calc.	24.86	4.66	1.79	31.87	–	–
	obs.	24.83	4.74	1.79	31.56	–	–
$(TBA)_2[(Mo_6Cl_8^i)Br_6^a]$	calc.	21.07	3.97	1.53	15.55	26.28	–
	obs.	21.22	3.96	1.53	15.32	26.53	–
$(TBA)_2[(Mo_6Cl_8^i)I_6^a]$	calc.	18.25	3.44	1.33	13.46	–	36.16
	obs.	18.14	3.43	1.44	13.62	–	36.50

5.5. Spectra

The IR spectra were measured on an NIC 7199 FT-IR spectrometer (Nicolet, Offenbach/Main, FRG) in pressed polyethylene. The Raman spectra were measured on a Cary 82 (Varian, Darmstadt, FRG) with an argon laser. The solids were measured as rotating samples at 80 K. About 20 mg of the pure substance pressed into the ring-shaped cavity (Ø = 8 mm, 1.75 mm wide) of a brass disk at 2 t cm^{-2} yielded a glass-like material [19, 20]. The degree of depolarization was determined using saturated solutions of the TBA salts in propylene carbonate at room temperature in rotating quartz cuvettes.

Acknowledgment

We would like to thank the Fonds der Chemischen Industrie for financial support.

References

1 H. Schäfer and H. G. von Schnering, *Angew. Chem.*, *76* (1964) 883.
2 H. Schäfer, C. Brendel, G. Henkel and B. Krebs, *Z. anorg. allg. Chem.*, *491* (1982) 275.
3 H. G. von Schnering, *Z. anorg. allg. Chem.*, *385* (1971) 75.
4 R. Mattes, *Z. anorg. allg. Chem.*, *357* (1968) 30.
5 F. A. Cotton, R. M. Wing and R. A. Zimmerman, *Inorg. Chem.*, *6* (1967) 11.
6 A. Zelverte, S. Mancour and P. Caillet, *Spectrochim. Acta A*, *42* (1986) 837.
7 D. Hartley and M. J. Ware, *Chem. Commun.*, (1967) 912.
8 J. C. Sheldon, *J. Chem. Soc.*, (1960) 1007.
9 H. Schäfer, H. Plautz, H.-J. Abel and D. Lademann, *Z. anorg. allg. Chem.*, *526* (1985) 168.
10 M. H. Chisholm, J. A. Heppert and J. C. Huffmann, *Polyhedron*, *3* (1984) 475.
11 H. G. von Schnering, W. May and K. Peters, *Z. Kristallogr.*, in press.
12 L. J. Guggenberger and A. W. Sleight, *Inorg. Chem.*, *8* (1969) 2041.
13 T. C. Zietlow, W. P. Schäfer, B. Sadeghi, N. Hua and H. B. Grau, *Inorg. Chem.*, *25* (1986) 2195.

14 W. Klemm, W. Bronger and H. G. von Schnering, Die neuere Entwicklung der Anorganischen Chemie mit einigen Beispielen aus der Chemie der Übergangselemente, *Jahrbuch 1966*, Landesamt für Forschung des Landes Nordrhein-Westfalen, Westdeutscher, Köln/Opladen, 1966, pp. 451–473.
15 K. Harder, G. Peters and W. Preetz, *Z. anorg. allg. Chem., 598–599* (1991) 139.
16 R. G. Woolley, *Inorg. Chem., 24* (1985) 3519.
17 G. Kliche and H. G. von Schnering, *Z. Naturf. B, 44* (1989) 74.
18 H. Schäfer, H. G. von Schnering, J. Tillack, F. Kuhnen, H. Wöhrle and H. Baumann, *Z. anorg. allg. Chem., 353* (1967) 281.
19 H. Homburg and W. Preetz, *Spectrochim. Acta A, 32* (1976) 709.
20 H. Homburg, *Z. anorg. allg. Chem., 460* (1980) 17.